ACS Catalysis

Research Article

pubs.acs.org/acscatalysis

X-ray Crystallography Reveals How Subtle Changes Control the Orientation of Substrate Binding in an Alkene Reductase

Yuri A. Pompeu, Bradford Sullivan, and Jon D. Stewart*

Department of Chemistry, University of Florida, 126 Sisler Hall, Gainesville, Florida 32611, United States

ABSTRACT: Reductions of (*S*)- and (*R*)-carvone by wild-type *Saccharomyces pastorianus* Old Yellow Enzyme (OYE 1) and a systematic collection of Trp 116 variants revealed that, for (*S*)-carvone, six Trp 116 mutants displayed inverted diastereoselectivity compared to the wild-type. For example, Ile and Val showed inverted stereoselectivity, but Leu and Phe maintained the wild-type stereopreference. For (*R*)-carvone, only two Trp 116 mutants (Ala and Val) reduced this alkene with reversed selectivity; all other catalytically active variants including Leu and Ile retained the wild-type diastereoselectivity. The same set of mutant enzymes was also used to catalyze the dehydrogenation of (*S*)- and (*R*)-carvone under aerobic conditions. To understand how small changes to the active site structure of OYE 1 could significantly influence its catalytic properties, we solved X-ray crystal structures of the wild-type as well as six key Trp 116 variants after individually soaking with both (*S*)- and (*R*)-carvone. In many cases, *pseudo*-Michaelis complexes formed *in crystallo*, and these revealed the details of protein−substrate interactions. Taken together, our results showed that the wild-type OYE 1 reduces carvone from a less preferred substrate binding orientation. The indole ring of Trp 116 physically blocks access to a hydrophobic active site pocket. Relieving the steric congestion by mutating Trp 116 allows entry of the isopropenyl side-chain of carvone into this hydrophobic pocket and also makes the opposite face of the π system accessible to hydride addition, thereby yielding the opposite diastereomer after net *trans*-addition of H_2.

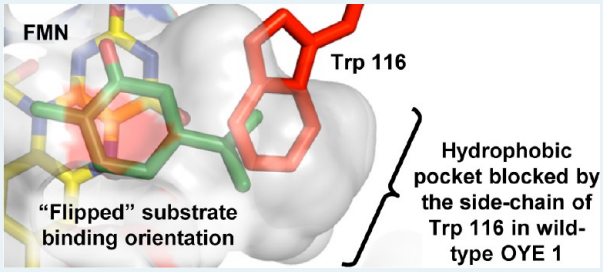

KEYWORDS: *alkene reductase, ene reductase, carvone, X-ray crystallography, binding orientation, mutant*

INTRODUCTION

Enzymes of the Old Yellow Enzyme (OYE) family have recently gained favor as stereoselective catalysts for reducing electron-deficient alkenes (for recent reports, see ref 1 and references therein). Reduction proceeds by a net *trans*-addition of H_2 to olefins,[2] particularly those conjugated with aldehydes, ketones, nitriles, nitro groups, and, in some cases, esters. Hydrogenation follows a polar mechanism in which hydride is transferred from reduced flavin mononucleotide (FMN) to the electron-deficient β-carbon with concomitant protonation at the α-carbon.[3] Both the stereochemical course and substrate range of OYEs complement those of most organometallic hydrogenation catalysts, which has led to a renewed interest in this class of flavoproteins, originally discovered in 1932 by Warburg.[4]

One challenge in developing biocatalytic methods for organic synthesis is that one enantiomer is often easily available, but the "other" enantiomer is not.[5] The very high stereoselectivities of OYEs are thus a double-edged sword that make it difficult to access both product stereoisomers unless the substrate structure can be altered, i.e., employing the opposite alkene configuration.[6] For example, wild-type *Saccharomyces pastorianus*[7] OYE 1 reduces simple α-alkyl-substituted 2-cyclohexenones, e.g., 2-methyl-2-cyclohexenone, to the corresponding (*R*)-products with very high stereoselectivities.[8] The same enzyme reduces both enantiomers of carvone to the analogous products (Scheme 1).[9] All of these reduction products derive from Michaelis complexes in which the 2-cyclohexenone ring can be superimposed on the aromatic ring carbons of *p*-hydroxybenzaldehyde, a potent OYE 1 inhibitor observed in the X-ray crystal structure of *S. pastorianus* OYE 1.[10] For simplicity, we refer to this arrangement as the "normal" substrate binding mode. With one exception (vide infra), we were unable to discover an enantiocomplementary OYE for any of the substrates we investigated and were therefore able to fulfill only half of our methodological goals. A more general solution to this problem is reported here that joins some additional successes in this area reported by other groups.[11]

In principle, one could either invert the stereoselectivity of an OYE by relocating the substrate from one side of the FMN cofactor to the other, or by turning the substrate over, thereby exposing the opposite face of the alkene π system to the FMN. Only the *si* face of the FMN cofactor is accessible in the active sites of OYEs, and prospects for remodeling the protein to accommodate substrate binding on the opposite face of the cofactor appeared bleak. We therefore concentrated on strategies to invert the orientation of substrate binding with respect to the FMN cofactor (referred to as "flipped" substrate binding, Scheme 1). The first steps toward achieving this goal came from a chance observation. Like many OYE family

Received: July 30, 2013
Revised: September 3, 2013
Published: September 9, 2013

   dx.doi.org/10.1021/cs400622e | *ACS Catal.* 2013, 3, 2376−2390

Scheme 1

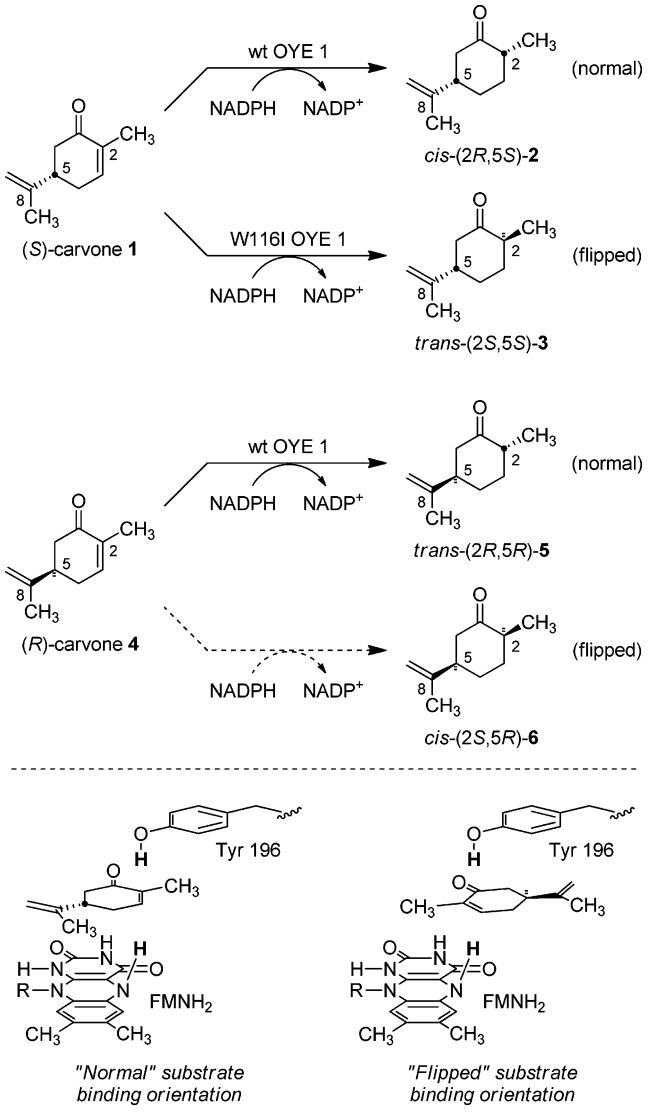

members,[12] wild-type OYE 1 contains Trp at position 116. Substituting Ile or Met at this position caused a nearly complete reversal of stereoselectivity toward (*S*)-carvone (Scheme 1).[13] Given the conservative nature of these amino acid changes, this was a surprising result. Data from ^{2}H NMR showed that, like the wild-type enzyme, the Trp 116 Ile mutant also catalyzed a net *trans*-addition of H_2, arguing that the reversed stereoselectivity was due to an alternative, "flipped" binding orientation that placed the opposite face of the alkene above the *si* face of the FMN cofactor. Interestingly, the same Trp 116 Ile mutant still reduced (*R*)-carvone to yield the product derived from the "normal" binding orientation.

While our earlier studies had yielded stereocomplementary OYE 1 variants for (*S*)-carvone reduction, this was an isolated example, and no solution for (*R*)-carvone was identified, at least in the limited number of Trp 116 replacements examined. More importantly, while we had deduced that (*S*)-carvone *should* have bound in the "flipped" orientation to explain the observed stereochemistry, we had no direct experimental evidence to support this contention. We therefore examined this system in more detail. Carvone has previously served as a useful test case in biocatalytic alkene reductions, which would allow comparison with previous studies in this area (see refs 1c,14 and references therein). Our goals were not only to solve the specific synthetic problems associated with carvone reductions, but also to discover general principles that might guide future efforts to adapt these versatile biocatalysts for even wider synthetic applications.

RESULTS AND DISCUSSION

A complete set of Trp 116 amino acid replacements for *S. pastorianus* OYE 1 was overexpressed in *Escherichia coli* as *N*-terminal glutathione *S*-transferase (GST) fusions and purified by affinity chromatography as described previously.[15] Since previous studies had shown that the tag had no significant impact on the properties of *S. pastorianus* OYE 1,[9] it was left in place for catalytic assays. Reductions of both (*S*)- and (*R*)-carvone were carried out individually using purified OYE 1 proteins for 16 h and substrate concentrations of 10 mM. NADPH was maintained in excess throughout the reactions by glucose oxidation mediated by glucose dehydrogenase. This equilibrium strongly favors products because gluconolactone spontaneously hydrolyzes, and this maintains the nicotinamide cofactor in the reduced form throughout the reaction. Relative conversions and product diastereomeric purities were determined by GC analysis using authentic standards used to assign both relative and absolute configurations.

Catalytic Studies of OYE 1 Mutants. *Reductions of (S)-carvone.* Replacements for Trp 116 had significant impacts on both the efficiency and the stereoselectivity of (*S*)-carvone reductions (Figure 1A). While most polar replacements, particularly those with charged side-chains, were highly detrimental, the majority of nonpolar amino substitutions yielded functional OYE 1 variants. The main exceptions were Asn and Gln, both of which gave good catalytic efficiencies and mainly the product expected to arise from "flipped" substrate binding. The most striking observation was that the Trp 116 Leu mutant afforded mostly the product derived from the "normal" substrate binding mode whereas the closely related amino acids Ile and Val gave almost exclusively the diastereomer derived from the "flipped" orientation. In addition, Thr, which is nearly isosteric with Val, gave much lower catalytic efficiency, although the stereoselectivity was almost completely reversed from that of wild-type. These were the first indications that substrate binding and catalytic activity could be altered by very subtle changes to the OYE 1 active site structure.

Reductions of (R)-carvone. Trp 116 substitution also had significant impacts on the outcomes of (*R*)-carvone reductions (Figure 1B). As before, polar amino acids (except for Asn and Gln) dramatically decreased alkene reduction efficiency. Surprisingly, all variants except two (Ala and Val) gave predominantly the product derived from the "normal" substrate binding mode. The behavior of the Val mutant is even more surprising since the closely related Leu and Ile variants productively bound (*R*)-carvone only in the "normal" orientation. From a practical point of view, the Ala and Val variants were useful in completing the collection of diastereoselective alkene reductases that allow selective access to all four stereoisomeric reduction products from (*S*)- and (*R*)-carvone (Scheme 1).

The results of carvone reduction by wild-type and Trp 116 variants of OYE 1 are summarized in Table 1. Successful replacements for Trp 116 can be divided into three categories based on their assumed substrate binding interactions prior to

dx.doi.org/10.1021/cs400622e | *ACS Catal.* 2013, 3, 2376−2390

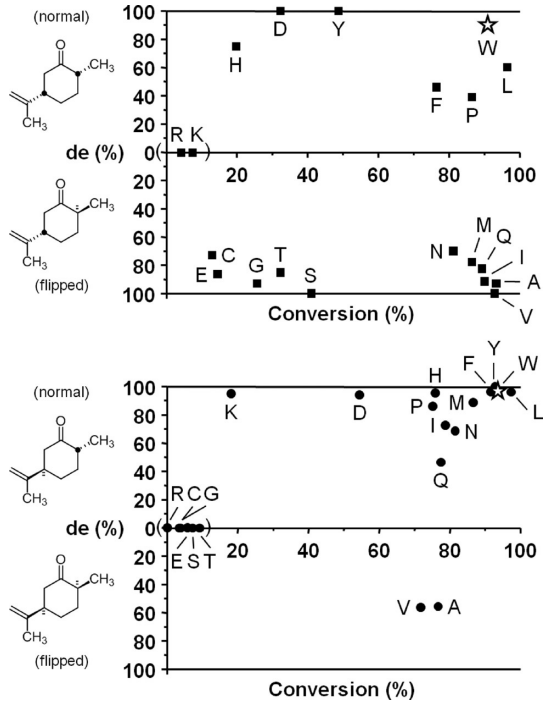

Figure 1. Carvone reduction by wild-type OYE 1 and Trp 116 variants. Reductions utilized purified GST-fusion proteins with NADPH maintained in excess by a cofactor regeneration system (glucose/glucose dehydrogenase). Reactions were incubated at room temperature for 16 h; then the extents of conversion and diastereomeric purities were assessed by GC/MS. Data for the wild-type enzyme are indicated by a star, and the identity of the amino acid at position 116 is shown next to the appropriate data point. (**A**) (*S*)-carvone data. (**B**) (*R*)-carvone data.

Table 1. Summary of Library Screening Results for Reductions of (*S*)- and (*R*)-carvone by OYE 1 and Trp 116 Variants[a]

Amino acid at position 116	(*S*)-carvone 1	(*R*)-carvone 4
Asp, His, Leu, Phe, Pro, Tyr, Trp (w.t.)	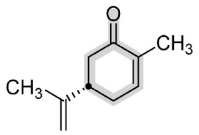	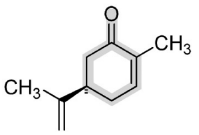
Asn, Gln, Ile, Met	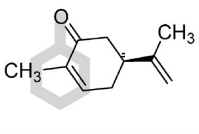	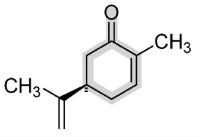
Ala, Val	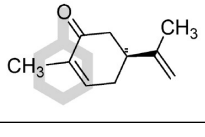	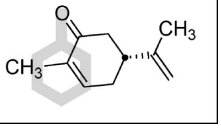

[a]The binding mode leading to the predominant product is depicted. The gray outline corresponds to the position of *p*-hydroxybenzaldehyde and indicates to the "normal" substrate binding mode. Amino acids that gave rise to little or no catalytic activity are excluded.[43]

hydride addition/protonation: (1) those that productively bound both (*S*)- and (*R*)-carvone mainly in the "normal" orientation; (2) those that bound (*S*)-carvone in a "flipped" orientation, but (*R*)-carvone in the "normal" fashion; (3) those that productively bound both (*S*)- and (*R*)-carvone in the "flipped" orientations.

As an additional probe of the active site environments of our OYE 1 variants, we also studied their ability to oxidize (*R*)- and (*S*)-carvone (Scheme 2). Dismutation predominates under anaerobic conditions in the absence of an external reductant such as NADPH or other electron acceptor. This process involves H_2 removal from one substrate molecule and subsequent transfer to a second.[2] Under aerobic conditions, molecular oxygen can compete with a second alkene molecule for electrons from reduced FMN; this alternative electron acceptor yields hydrogen peroxide and eliminates formation of the dihydrocarvone byproduct. Regardless of the ultimate fate of the electrons, OYE 1-mediated oxidations of 2-cyclohexenones are essentially irreversible since the initially formed cyclohexadienones rapidly tautomerize to the corresponding phenol. These phenols subsequently form high-affinity charge-transfer complexes with OYE 1 that feature absorbance maxima at about 650 nm.[16] These complexes can also be recognized visually by the change in enzyme color from bright yellow (oxidized FMN form) to green.

As the microscopic reverse of the alkene reduction process, carvone oxidation requires that the reacting hydrogens be oriented in a *trans*-diaxial arrangement (Scheme 2). Because the location of the FMN is fixed within the protein environment, the substrate must be positioned so that its C_β hydrogen lies within the cofactor's cone of reactivity above N_5.[17] In addition, the carbonyl oxygen must form hydrogen bonds to the side-chains of His 191 and Asn 194 to facilitate the polar elimination of H_2. These requirements, in addition to avoiding steric conflict between the isopropenyl side-chain and the FMN cofactor, define the active site locations of (*S*)- and (*R*)-carvone to be those shown in Scheme 2. While the ring carbons of (*S*)-carvone lie in the same locations as those of a phenol inhibitor for the dehydrogenation step, those of (*R*)-carvone must be shifted somewhat to maintain the proper locations of C_β and the carbonyl oxygen. This has the effect of moving the (*R*)-substrate into closer proximity to the side-chain of the amino acid at position 116 as compared to its (*S*)-counterpart. For this reason, we anticipated that the nature of the amino acid at position 116 might influence the efficiency of carvone oxidations, particularly for the (*R*)-enantiomer.

The oxidation activities of OYE 1 Trp 116 variants toward both (*S*)- and (*R*)-carvone were determined spectrophotometrically for all mutants with reasonable alkene reduction efficiencies.[18] Because phenol **7** is a potent inhibitor of OYE 1, progress curves for these reactions are inherently nonlinear. We therefore chose a fixed reaction time (24 h) and assessed the fraction of enzyme with bound phenol **7** as an index of relative carvone oxidation efficiency (Figure 2). This involved measuring the A^{462}/A^{648} ratios at the start of the reaction and after 24 h since these wavelengths correspond to λ_{max} values for FMN in the absence of phenol **7** and the charge-transfer band, respectively. End point values for completely phenol-complexed proteins were measured by adding an excess of *p*-chlorophenol in separate experiments.[19] These data allowed the fractional saturation for each dismutation reaction to be calculated after 24 h (Figure 2).[20] As anticipated, there was a correlation between the size of the side-chain at position 116 and the efficiency of carvone oxidation, and (*S*)-carvone was more readily accepted than the (*R*)-antipode.

Crystallographic studies. To better understand the molecular interactions that control the orientation of substrate

dx.doi.org/10.1021/cs400622e | *ACS Catal.* 2013, 3, 2376−2390

Scheme 2

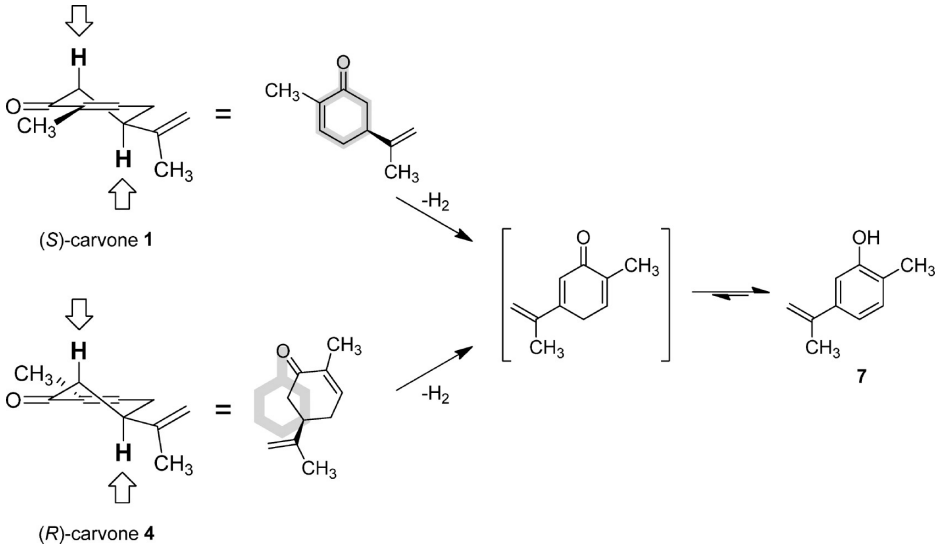

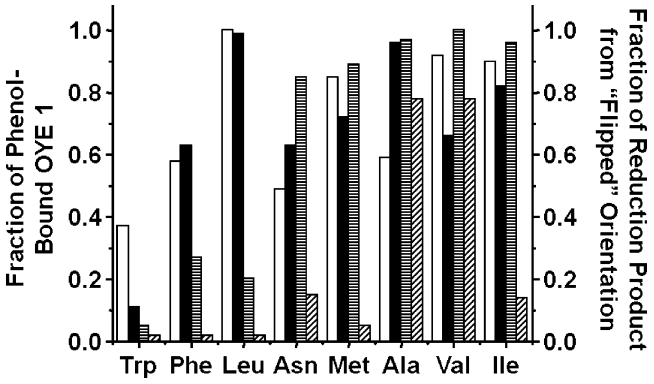

Figure 2. Catalytic efficiencies of wild-type OYE 1 and Trp 116 variants for carvone oxidation and reduction. Wild-type OYE 1 and selected Trp 116 mutants were incubated with either (*S*)- or (*R*)-carvone under aerobic conditions in the absence of external reductant, then the fraction of protein complexed with phenol **7** was determined spectrophotometrically (white and black bars, respectively). For comparison, the fraction of (*S*)- and (*R*)-carvone reduction products derived from the "flipped" binding orientation are also shown (horizontal- and diagonally striped bars, respectively).

binding to wild-type OYE 1 and its Trp 116 variants, we determined the three-dimensional structures for key mutants in the presence of substrates and/or other ligands using X-ray crystallography (Tables 2−5). To avoid potential interference during crystallization, the GST fusion tag was deleted and proteins were isolated by affinity chromatography on a phenol-derivatized resin[21] with final purification by gel filtration. All variants crystallized under very similar conditions and in the same space group as reported by Fox and Karplus for the wild-type enzyme (P 4_3 2_1 2).[10] As expected, the overall structures for all mutants were nearly identical (RMSD 0.10−0.27 Å). The only exception was the extra-barrel helix B (residues 145−153), which exhibited greater deviation. These variations were usually correlated with small changes in the unit cell dimensions, suggesting that crystal packing forces were responsible. All structures were solved by molecular replacement using the wild-type OYE 1 (PDB code 1OYB),[10,22] or a Trp 116 Ile variant solved in conjunction with an earlier study (PDB code 3RND).[15] The positions of the mutant side-chains at position

Table 2. Crystallography Data Collection and Refinement Statistics (Accession Codes: 4GXM, 4GWE, 4H6K)

accession code	4GXM	4GWE	4H6K
position 116 a.a.	Leu	Leu	Ile
ligand soaked	(*R*)-carvone	(*R*)-carvone	(*R*)-carvone
observed active site ligand	oxidation product **7** (from (*R*)-carvone)	(*R*)-carvone	Chloride or water
ligand orientation	"normal"	"normal"	
X-ray source	NSLS beamline X26C	NSLS beamline X26C	NSLS beamline X25
space group	P 4_3 2_1 2	P 4_3 2_1 2	P 4_3 2_1 2
unit cell dimensions			
a = *b*, *c* (Å)	141.12, 42.92	140.78, 42.76	140.93, 42.46
resolution (Å)[a]	34.2−1.36 (1.41−1.36)	28.2−1.45 (1.49−1.44)	31.5−1.55 (1.60−1.55)
unique reflections	87,060 (5,990)	70,039 (4,324)	62,517 (6,122)
completeness (%)	93.78 (65.40)	90.83 (56.74)	99.94 (99.69)
multiplicity	16.5 (7.5)	12.8 (11.7)	9.1 (8.7)
R_{sym}[b]	0.062 (0.38)	0.044 (0.18)	0.080 (0.90)
I/σ (I)	39.89 (4.49)	48.82 (12.97)	14.22 (1.89)
R_{work}[c], R_{free}[d]	0.108, 0.137	0.115, 0.145	0.182, 0.204
Ramachandran statistics[e]			
favored (%)	98	98	97
allowed (%)	2	2	3
outliers (%)	0	0	0
number of protein, solvent and ligand atoms	3,287, 633, 100	3,255, 590, 65	3,216, 313, 56
average B factors (Å^2)			
protein	11.5	13	29.6
solvent	25.4	26.7	38
FMN	7.5	10.0	19.5
ligands	18.1	19.1	

[a]Values in parentheses denote data for the highest resolution bin. [b]$R_{merge} = \sum|I - \langle I\rangle|/\sum\langle I\rangle$. [c]$R_{work} = \sum||F_o(hkl)| - |F_c(hkl)||/\sum|F_o(hkl)|$. [d]$R_{free}$ is calculated in the same manner as R_{work} using 10% of the reflection data not included during the refinement. [e]Statistics generated using MOLPROBITY. [44]

dx.doi.org/10.1021/cs400622e | *ACS Catal.* 2013, 3, 2376−2390

Table 3. Crystallography Data Collection and Refinement Statistics (Accession Codes: 4GE8, 4GBU, 4K7V)

accession code	4GE8	4GBU	4K7V
position 116 a.a.	Ile	Ala	Ala
ligand soaked	(*S*)-carvone	(*S*)-carvone	(+)-dihydrocarvone
observed active site ligand	(*S*)-carvone	oxidation product 7 (from (*S*)-carvone)	(*R*)-carvone
ligand orientation	"flipped"	"flipped"	flipped
X-ray source	NSLS beamline X25	NSLS beamline X6A	NSLS beamline X6A
space group	P 4_3 2_1 2	P 4_3 2_1 2	P 4_3 2_1 2
unit cell dimensions			140.85, 42.84
$a = b$, c (Å)	140,93, 42.48	141.12, 42.81	
resolution (Å)[a]	24.2−1.5 (1.55−1.49)	21.0−1.18 (1.22−1.17)	35.42−1.52 (1.57−1.516)
unique reflections	68,916 (6,757)	141,261 (13,929)	66,315 (6,492)
completeness (%)	99.75 (99.22)	99.71 (99.59)	98.52 (97.79)
multiplicity	11.1 (10.4)	7.1 (6.6)	7.8 (7.2)
R_{sym}[b]	0.048 (0.63)	0.076 (0.55)	0.093 (0.524)
I/σ (I)	29.40 (2.83)	15.10 (2.05)	22.67 (3.44)
R_{work}[c], R_{free}[d]	0.137, 0.170	0.100, 0.121	0.145, 0.183
Ramachandran statistics[e]			
favored (%)	98	98	97
allowed (%)	2	2	3
outliers (%)	0	0	0
number of protein, solvent and ligand atoms	3,256, 465, 91	3,281, 658, 107	3,205, 500, 62
average B factors (Å^2)			
protein	21.2	11.5	18.5
solvent	38.0	26.1	30.90
FMN	13.7	6.9	16.6
ligands	23.9	16.3	25.3

[a]Values in parentheses denote data for the highest resolution bin. [b]$R_{merge} = \sum|I - \langle I\rangle|/\sum\langle I\rangle$. [c]$R_{work} = \sum|F_o\ (hkl)| - |F_c\ (hkl)|/\sum|F_o\ (hkl)|$. [d]$R_{free}$ is calculated in the same manner as R_{work} using 10% of the reflection data not included during the refinement. [e]Statistics generated using MOLPROBITY. [44]

Table 4. Crystallography Data Collection and Refinement Statistics (Accession Codes: 4K8E, 4H4I, 4K8H)

accession code	4K8E	4H4I	4K8H
position 116 a.a.	Val	Val	Val
ligand soaked	(*R*)-carvone	(*S*)-carvone	(+)-dihydrocarvone
observed active site ligand	oxidation product 7 (from (*R*)-carvone)/ chloride[f]	oxidation product 7 (from (*S*)-carvone)	(*R*)-carvone
ligand orientation	flipped	"flipped"	flipped
X-ray source	NSLS beamline X6A	NSLS beamline X6A	NSLS beamline X6A
space group	P 4_3 2_1 2	P 4_3 2_1 2	P 4_3 2_1 2
unit cell dimensions	141.35, 42.85		141.443, 42.851
$a = b$, c (Å)		141.00, 42.82	
resolution (Å)[a]	24.2−1.27 (1.315−1.269)	23.6−1.25 (1.29−1.25)	35.48−1.55 (1.605−1.55)
unique reflections	113,485 (11,067)	119,164 (11.776)	65,589 (6,247)
completeness (%)	99.44 (98.44)	99.98 (99.95)	99.95 (99.57)
multiplicity	9.9 (9.0)	10.2 (9.9)	12.2 (12.2)
R_{sym}[b]	0.069 (0.547)	0.10 (0.55)	0.086 (0.676)
I/σ (I)	20.33 (2.46)	19.58 (3.07)	24.60 (3.79)
R_{work}[c], R_{free}[d]	0.107, 0.127	0.124, 0.146	0.124, 0.162
Ramachandran statistics[e]			
favored (%)	98	98	97
allowed (%)	2	2	3
outliers (%)	0	0	0
number of protein, solvent and ligand atoms	3,325, 642, 97	3,286, 660, 108	3,320, 542, 72
average B factors (Å^2)			
protein	11.7	9.8	15.00
solvent	27.90	26.5	27.60
FMN	8.6	5.8	12.1
ligands	16.6	14.7	19.3

[a]Values in parentheses denote data for the highest resolution bin. [b]$R_{merge} = \sum|I - \langle I\rangle|/\sum\langle I\rangle$. [c]$R_{work} = \sum|F_o\ (hkl)| - |F_c\ (hkl)|/\sum|F_o\ (hkl)|$. [d]$R_{free}$ is calculated in the same manner as R_{work} using 10% of the reflection data not included during the refinement. [e]Statistics generated using MOLPROBITY. [44] [f]Occupancies of phenol 7 and chloride were ca. 1: 1 in this structure.

dx.doi.org/10.1021/cs400622e | ACS Catal. 2013, 3, 2376−2390

Table 5. Crystallography Data Collection and Refinement Statistics (Accession Codes: 3TXZ, 4K7Y)

accession code	3TXZ	4K7Y
position 116 a.a.	Gln	Thr
ligand soaked	(*R*)-carvone	(*R*)-carvone
observed active site ligand	(*R*)-carvone	chloride
ligand orientation	unique	
X-ray source	NSLS beamline X25	NSLS beamline X6A
space group	P 4_3 2_1 2	P 4_3 2_1 2
unit cell dimensions		
a = *b*, *c* (Å)	141.36, 42.69	141.37, 42.83
resolution (Å)[a]	45.0−1.7 (1.76−1.7)	23.59−1.2 (1.242−1.199)
unique reflections	48,165 (4,726)	135,136 (13,135)
completeness (%)	99.99 (99.96)	99.80 (98.28)
multiplicity	9.5 (6.2)	6.0 (5.6)
R_{sym}[b]	0.052 (0.58)	0.067 (0.570)
I/σ (I)	17.10 (2.22)	14.34 (1.87)
R_{work}[c], R_{free}[d]	0.161, 0.186	0.1150, 0.1350
Ramachandran statistics[e]		
favored (%)	98	97
allowed (%)	2	3
outliers (%)	0	0
number of protein, solvent and ligand atoms	3,244, 368, 43	3,358, 666, 58
average B factors (Å^2)		
protein	23.5	11.4
solvent	36.1	26.40
FMN	16.8	8.3
ligands	25.6	

[a]Values in parentheses denote data for the highest resolution bin. [b]$R_{merge} = \sum|I - \langle I\rangle|/\sum\langle I\rangle$. [c]$R_{work} = \sum|F_o\ (hkl)| - |F_c\ (hkl)|/\sum|F_o\ (hkl)|$. [d]$R_{free}$ is calculated in the same manner as R_{work} using 10% of the reflection data not included during the refinement. [e]Statistics generated using MOLPROBITY. [44]

116 were readily apparent from the high-resolution electron density difference maps.

Soaking experiments were carried out by adding neat (*R*)- and (*S*)-carvone to pregrown crystals in the mother liquor prior to mounting.[23] We also carried out some soaking experiments with (+)-dihydrocarvone,[24] which was added to crystals of the Thr, Ala, and Val OYE 1 variants. All crystals initially exhibited the characteristic bright yellow color of oxidized flavin; however, after several days of soaking in the presence of carvone, some mutants gradually adopted a green color. This was particularly apparent in crystals of the Val and Ala replacements. By contrast, crystals of the Ile and Gln variants remained bright yellow, even after prolonged soaking times. When ligands were observed in the active site, occupancies were generally very high (≥85%), and their locations were very well-defined by the electron density. Ligand atoms were added manually after the protein, and most water molecules had been refined to avoid model bias.

Wild-Type. Crystals of wild-type OYE 1 were soaked individually with both (*S*)- and (*R*)-carvone and complete, high-resolution data sets were collected for both experiments.[25] No electron density that corresponding to carvone was observed; instead, the spherical electron density lying above the FMN and near the side-chains of His 191 and Asn 194 was well-fit by a chloride ion. Its position was essentially the same as that occupied by the phenolate oxygen in charge-transfer complex structures such as those reported by Fox and Karplus.[26] Chloride was present at about 220 mM in the crystallization buffer and binds to wild-type OYE 1 with a K_D value of 8 mM, making it the "default" active site ligand in the absence of other additives.[27] That it remained bound to the wild-type enzyme even in the presence of saturating carvone implies that the thermodynamic stabilities of these complexes were insufficient to displace an active site ligand with relatively modest affinity. It is also possible that loop 6 (residues 289−309) cannot be repositioned to accommodate the carvone isopropenyl group in a wild-type active site.

Trp 116 Leu Mutant. Based on the stereochemistry of the carvone reduction products obtained from this protein, we surmised that the Trp 116 Leu OYE 1 variant must have bound both (*R*)- and (*S*)-carvone in the "normal" orientation. Numerous soaking experiments were carried out in an effort to observe (*S*)-carvone within the active site; unfortunately, only a spherical region of electron density best modeled as a chloride ion was found when this ligand was used. By contrast, we were successful with (*R*)-carvone, although the nature of the active site ligand depended on the time between substrate addition and flash cooling the crystals in liquid nitrogen (Figure 3). Initially yellow crystals gradually became green after soaking with (*R*)-carvone for 2 days at about 4 °C (Figure 3A). When the soaking time was decreased to 2.5 h before freezing in liquid nitrogen, the crystals remained yellow (Figure 3A). These color changes suggested that the green crystals contained the phenolic oxidation product **7** derived from (*R*)-carvone while the yellow crystals contained unmodified (*R*)-carvone. To test this hypothesis, we carried out *in crystallo* UV−vis spectroscopy during X-ray data collection. In these experiments, single crystals of the Trp 116 Leu mutant that had been soaked in (*R*)-carvone for different times were mounted for X-ray data collection at 100 K in the normal fashion. After determining the optimal crystal orientation, UV−vis absorbance spectra between 350 and 800 nm were collected using a microspectrophotometer that was focused on the crystal rotation axis. Complete data sets were collected for both (yellow and green) crystal forms, which exhibited significantly different absorbance spectra in the 550−800 nm (Figure 3B).

As expected from the results of *in crystallo* spectroscopy, the X-ray structure of the green crystals of (*R*)-carvone-soaked Trp 116 Leu had ligand electron density that was best fit by phenol **7**, rather than the starting (*R*)-carvone (Figure 3C, PDB code 4GXM). Since no free phenols were present during the purification procedure or in the crystallization buffer, we concluded that carvone oxidation must have occurred post crystallization. The orientation of phenol **7** in the active site matched our expectations for the "normal" binding mode and also superimposed very well on the previously observed *p*-hydroxybenzaldehyde structure.[10] This location placed the ligand's isopropenyl moiety very close to the side-chain of Phe 296, which is part of loop 6 (closest approach of 3.20 Å). Despite this proximity, Phe 296 predominantly occupied one well-defined conformation (Figure 3C). The Leu side-chain at position 116 was also well-defined with no unduly close contacts between the methyl group of **7** and this protein residue.

Both the ligand electron density from the yellow crystals of (*R*)-carvone soaked Trp 116 Leu OYE 1 and the absence of an *in crystallo* absorption band in the 500−800 nm range were consistent with unmodified substrate in the active site (Figure 3D; PDB code 4GWE). (*R*)-Carvone was easily identifiable in

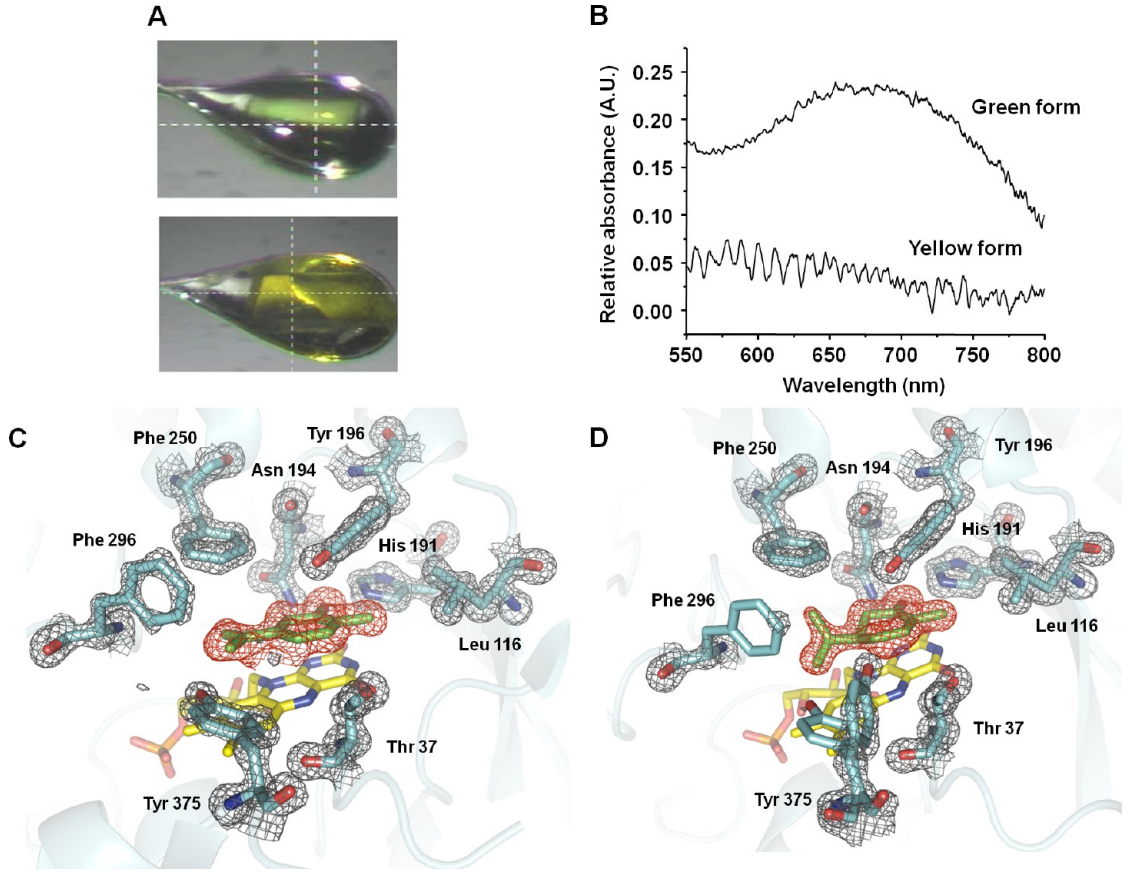

Figure 3. Structural studies of the Trp 116 Leu variant of OYE 1. (**A**) Protein crystals soaked with (*R*)-carvone for several days prior to storage at 77 K yielded green crystals (top) while those soaked for only a few minutes prior to flash cooling and X-ray data collection were yellow (bottom). (**B**) *In crystallo* UV−vis spectra of green and yellow crystals collected during X-ray irradiation. While the yellow crystals were featureless in the 550−800 nm region, the green crystals exhibited a peak with λ_{max} at about 660 nm, consistent with a phenol(ate) charge transfer complex in the active site. (**C**) X-ray structure of phenol **7** bound to Trp 116 Leu OYE 1 in the "normal" orientation (green crystal form, PDB code 4GXM). Electron density maps (2mFo-DFc) for key active site residues are shown in gray mesh at the 1.2 σ contour level. Carbon atoms are colored cyan for protein residues, yellow for FMN and green for phenol **7**. An omit difference map (mFo-DFc) is shown in red mesh for the ligand at the 3.0 σ contour level. (**D**) X-ray structure of (*R*)-carvone bound to Trp 116 Leu OYE 1 in the "normal" orientation (yellow crystal form, PDB code 4GWE). Atom and map colors are the same as those as in Figure 3C.

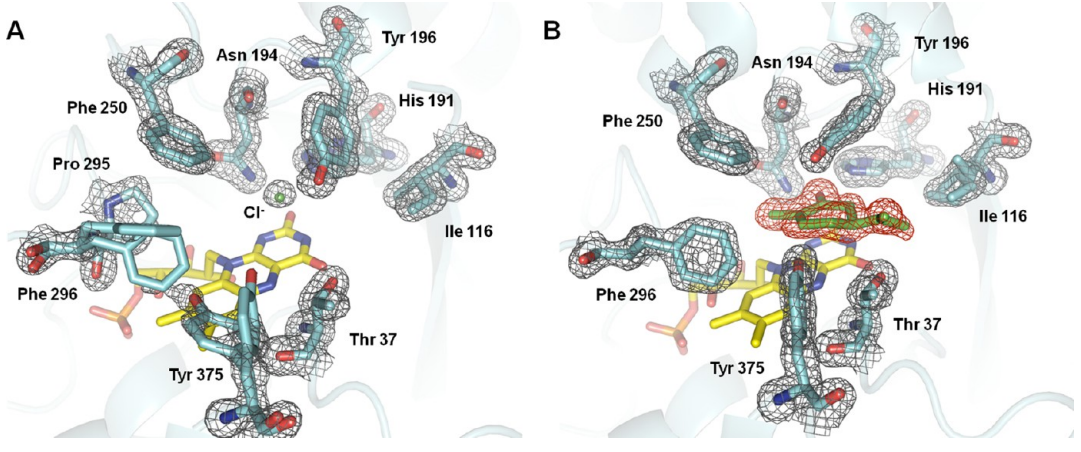

Figure 4. Trp 116 Ile OYE 1 structures. (**A**) The X-ray structure from crystals soaked with (*R*)-carvone showed no identifiable active site electron density apart from a sphere that could be modeled as chloride (PDB code 4H6K). Atom colors are the same as those as in Figure 3C. The gray mesh represents the 2mFo-DFc map contoured at the 1.0 σ level for key protein residues while the red mesh depicts the mFo-DFc omit map at the 3 σ contour level for the ligand. The side-chains of Phe 296 and Tyr 375 were found in multiple conformations, and the best fits to the observed electron density are shown. (**B**) X-ray structure of (*S*)-carvone-soaked crystals (PDB code 4GE8). Atom and map colors are the same as those in panel **A**. The major conformation of Ile 116 showed a 180° χ_1 rotation from its orientation in the chloride complex, and at least two conformers were observed in the crystal structure. By contrast, the side-chains of Phe 296 and Tyr 375 were well-defined.

dx.doi.org/10.1021/cs400622e | *ACS Catal.* 2013, 3, 2376−2390

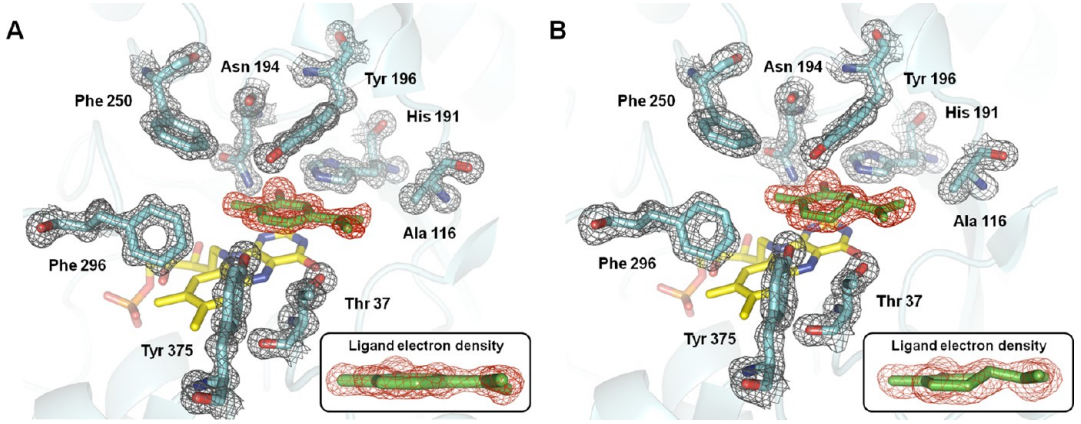

Figure 5. Structures of Trp 116 Ala OYE 1 soaked with (*S*)-carvone and (+)-dihydrocarvone. (**A**) Complex with phenol **7** in the "flipped" orientation formed after soaking for an extended time with (*S*)-carvone (PDB code 4GBU). Atom colors are the same as those in Figure 3C. The gray mesh represents the 2mFo-DFc map contoured at the 1.2 σ level for key protein residues while the red mesh depicts the mFo-DFc omit map at the 3 σ contour level for the ligand. The inset shows the ligand electron density whose shape is consistent with oxidation product **7**. (**B**) Complex with (*R*)-carvone observed after overnight soaking with (+)-dihydrocarvone (PDB code 4K7V). Atom and map colors are the same as those in panel **A**. The inset shows the ligand electron density whose shape is consistent with (*R*)-carvone **4**.

the experimental electron density maps, and the ligand was bound in the active site approximately parallel to the isoalloxazine ring of the FMN. As in the previous structure, the ligand was found in the "normal" binding mode and the positions of bound phenol **7** and (*R*)-carvone **4** were very similar. The ring carbons of **4** also superimposed well on those of *p*-hydroxybenzaldehyde complexed to wild-type OYE 1.[10] The carbonyl oxygen of **4** was ideally positioned to form hydrogen bonds with both *Nε*2 of His 191 and *Nδ*2 of Asn 194. Its isopropenyl group pointed away from the side chain of Leu 116 and made contacts with the side-chains of Phe 250, Pro 295, and Phe 296. The side chain of the latter showed the largest movement to accommodate the ligand, rotating nearly 90° around χ_2 along with a 0.35 Å backbone movement. Minor adjustments were also observed in the side-chain positions of Phe 250 and Tyr 375, with the latter occupying multiple conformations. The C_2 methyl group of **4** appeared to make hydrophobic contacts with *Cδ*1 and *Cδ*2 of Leu 116.

The distance and angle from the FMN N_5 atom and the plane of the isoalloxazine ring (3.75 Å and 105°, respectively) suggests that this complex mimics the catalytically productive Michaelis complex in the "normal" binding orientation. Two changes in protein structure were apparent when the (*R*)-carvone **4** and phenol **7** complexes were compared. First, the electron density for the side-chain of Phe 296 was weak in the presence of **4**, and it was clear that several conformations were present in the ensemble of protein molecules within the crystal (Figure 3D). Second, both the backbone and the side-chain of Tyr 375 were also found in at least two conformations. These observations suggest that additional changes at positions 296 and 375 that create additional space for substrate binding might yield even more catalytically efficient OYE 1 variants. The close approach of the isopropenyl group to the above-mentioned protein residues may also explain why we were unable to observe a complex with (*S*)-carvone despite numerous soaking attempts. While the isopropenyl side-chains occupy similar locations in the two carvone enantiomers, their exact locations differ slightly, and in cases where they are nearly in van der Waals contact with protein residues, very minor changes in the location of this moiety may have significant impacts.

Trp 116 Ile Mutant. Soaking this mutant with (*R*)-carvone failed to yield active site electron density that could be assigned as carvone; instead, only chloride ion was found (Figure 4A, PDB code 4H6K). This high-resolution structure (1.55 Å) showed very well-defined electron density for all atoms of the Ile 116 side-chain (Figure 4A), while the side-chains of Phe 296 and Tyr 375 showed indications of disorder, with weak electron density and high B-factors. As anticipated, this substitution created a much larger pocket on the "eastern" side of the OYE 1 active site just below Tyr 196.

The addition of (*S*)-carvone to these crystals yielded a *pseudo*-Michaelis complex that demonstrated directly—for the first time—that carvone could be accommodated in the active site of *S. pastorianus* OYE 1 in a "flipped" orientation. (Figure 4B, PDB code 4GE8). The side-chain of Tyr 196 moved significantly to bind the substrate, exhibiting a χ_2 rotation of 80° and a slight backbone shift. These shifts would favor Tyr 196-mediated proton transfer to the α-carbon of an enol(ate) intermediate. (*S*)-Carvone was stacked above the FMN cofactor with its carbonyl oxygen atom positioned to form hydrogen bonds with both *Nε*2 of His 191 and *Nδ*2 of Asn 194. Its isopropenyl group occupied a hydrophobic pocket directly above Thr 37 and made hydrophobic contacts with the side chain of the Ile introduced at position 116. The side-chains of Phe 296 and Tyr 375 showed well-defined electron density, in contrast to this region in the uncomplexed enzyme. The distance and angle from N_5 of the plane of the FMN (3.70 Å and 89°, respectively) were within the range of values expected[17] for catalytically relevant complex.

Interestingly, the side-chain of Ile 116 was no longer well-defined at the methyl terminus in this *pseudo*-Michaelis complex; rather, two different conformations were observed at the point of closest approach to the bound substrate (Figure 4B). In one (occupancy ca. 0.45), the side-chain showed a 180° rotation about χ_1 to avoid clash with the isopropenyl side-chain of (*S*)-carvone. The other Ile 116 conformer (occupancy ca. 0.55) matched that observed in the chloride complex described above. This behavior suggests that there may be some steric interference between the substrate and the residue at position 116, even in a variant that allows the substrate to bind in the "flipped" orientation. The almost-too-close approach between

dx.doi.org/10.1021/cs400622e | *ACS Catal.* 2013, 3, 2376−2390

Scheme 3

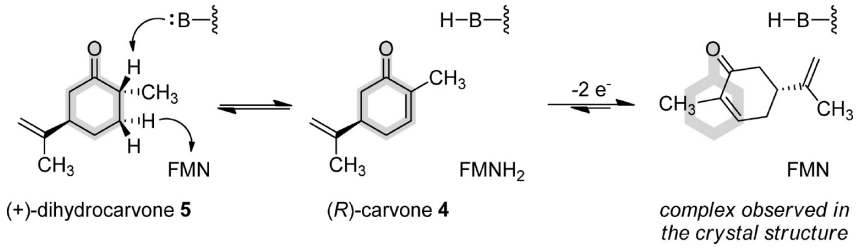

the side-chain of Ile at position 116 and the isopropenyl moiety of the substrate may also explain why the same mutant was unable to bind (*R*)-carvone in an analogous "flipped" orientation. As noted above, the side-chains of these substrate enantiomers occupy similar, but not identical, spatial positions.

Trp 116 Ala Mutant. Based on the reduction products, we deduced that the Trp 116 Ala mutant must have bound both (*S*)- and (*R*)-carvone primarily in "flipped" orientations. These predictions were borne out by the results of soaking experiments, which yielded electron density maps that were only consistent with the expected ligand binding orientation (Figure 5). Unfortunately, the high dismutation activity of this OYE 1 variant toward both carvone enantiomers meant that only phenol **7** could be observed in the crystals, even after relatively short soaking times (Figure 5A, PDB code 4GBU[28]). The position of phenol **7** in both complexes was very similar to that observed for the (*S*)-carvone/Trp 116 Ile variant and also close to that observed for the Val structures (vide infra), although C_8 of the ligand was shifted by 0.64 Å to make contact with the C_β atom of the Ala at position 116.

Soaking crystals of the Trp 116 Ala mutant with (+)-dihydrocarvone **5** overnight at 4 °C yielded active site electron density best fit by (*R*)-carvone **4** in the flipped orientation (Figure 5B, PDB code 4K7V). Attempts to fit the ligand electron density with fully dismutated product **7** or (+)-dihydrocarvone yielded much poorer results (data not shown). One possible route to the crystallographically observed complex is summarized in Scheme 3. *Trans*-elimination of H_2 from **5** would most logically occur from a binding arrangement in which the substrate's ring atoms matched those of the phenol inhibitor, thereby yielding reduced cofactor and (*R*)-carvone within the active site in the "normal" orientation. From this complex, the $FMNH_2$ can either transfer a pair of electrons to the alkene (back-reaction to reform **5**) or reduce a different acceptor (likely O_2) in an essentially irreversible step. This would leave an oxidized substrate in the active site with an oxidized cofactor. In the absence of an external reductant, this dead-end complex then isomerized to the favored "flipped" binding orientation to yield the crystallographically observed complex.[29] One puzzling observation is that little or no further dismutation of (*R*)-carvone to phenol **7** was observed in the crystal structure, despite the demonstrated ability of this mutant to catalyze this reaction when (*R*)-carvone was the starting substrate. It is possible that the enzyme had insufficient time to carry out the second dismutation step prior to flash cooling.

Regardless of the precise mechanism by which the "flipped" (*R*)-carvone complex with the Trp 116 Ala mutant was formed, this structure provided valuable information. The initial dehydrogenation step most likely involved the "normal" substrate binding mode, clearly demonstrating that this mutant is capable of interacting with substrate in this manner (Scheme 3). That the final, crystallographically observed (*R*)-carvone complex involved the "flipped" orientation showed that this arrangement is energetically preferred even when the alternative is accessible. This led us to hypothesize that OYE 1 intrinsically prefers to bind carvone in the "flipped" orientation and only when this arrangement is sterically precluded by an amino acid side-chain at position 116 is the "normal" binding orientation utilized. This notion was further supported by studies of the Trp 116 Val mutant.

Trp 116 Val Mutant. Like the Ala variant, Val substitution at position 116 resulted in carvone reduction products presumed to arise from the "flipped" substrate binding orientation. Crystals of the Trp 116 Val mutant were soaked with both (*R*)- and (S)-carvone, and complete data sets were collected for both experiments (PDB codes 4K8E and 4H4I, respectively). In both cases, carvone oxidation product **7** was found in the active site, and as expected, both structures were essentially identical. The isopropenyl group of **7** made hydrophobic contacts with both Cγ1 and Cγ2 of the Val at position 116 and the phenolic oxygen made short (2.71 and 2.77 Å) and well aligned hydrogen bonds with Nε2 of His 191 and Nδ2 of Asn 194 (data not shown).

Soaking the Trp 116 Val mutant with (+)-dihydrocarvone **5** yielded electron density that could be partially accounted for by (*R*)-carvone in the "flipped" binding orientation (PDB code 4K8H). This ligand likely arises by the same mechanism as described above for the Ala case (Scheme 3) and further demonstrates that even when both ligand binding orientations are accessible, OYE 1 prefers the "flipped" arrangement. In the case of the Val variant, however, it appeared that the crystals contained a mixed population of ligand with both (*R*)-carvone and phenol **7** present.

Trp 116 Thr Mutant. The Thr mutant was chosen for additional study because this residue is nearly isosteric with Val (though very different in polarity). Our hypothesis was that if substrate binding orientation was controlled solely by steric factors, the Thr and Val variants should show similar properties. This was not observed. Substituting Thr for Trp 116 was highly detrimental for the catalytic efficiency of OYE 1, and this mutant showed essentially no conversion for (*R*)-carvone and relatively poor conversion of (*S*)-carvone (with reversed stereoselectivity; Figure 1).

We soaked crystals of the Thr variant individually with (*S*)- and (*R*)-carvone as well as (+)-dihydrocarvone and collected complete, high-resolution data sets for all three experiments. In all cases, no active site electron density beyond that of chloride (the "default" ligand always found in nonsoaked crystals of OYE 1) was observed. The highest resolution structure (1.2 Å) was derived from soaking with (*R*)-carvone (PDB code 4K7Y).[30] Surprisingly, the side-chain of Asn 194 appeared to occupy at least two different conformations in this structure with an approximate occupancy of 65: 35. To the best of our knowledge, this phenomenon has not been observed in any

dx.doi.org/10.1021/cs400622e | *ACS Catal.* 2013, 3, 2376−2390

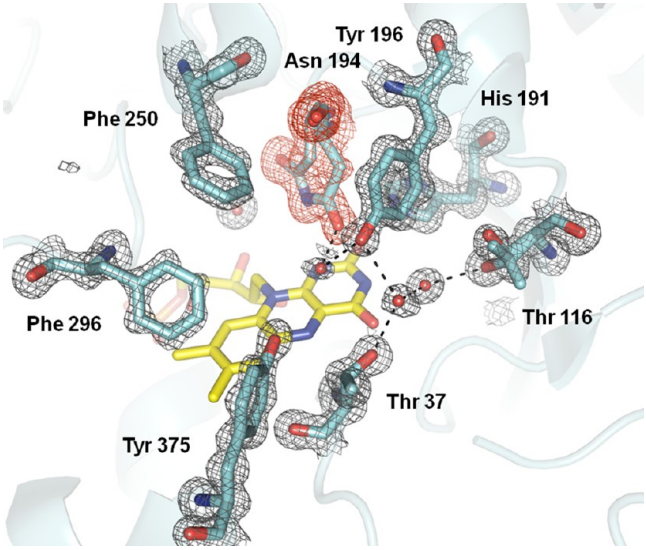

Figure 6. Structure of Trp 116 Thr OYE 1. The gray mesh shows the 2mFo-DFc electron density map contoured at the 1.2 σ level for key protein residues. The red mesh shows the omit mFo-DFc maps at the 3 σ level for the ligand. Protein residues are colored in cyan, FMN in yellow, and the waters are shown as red spheres.

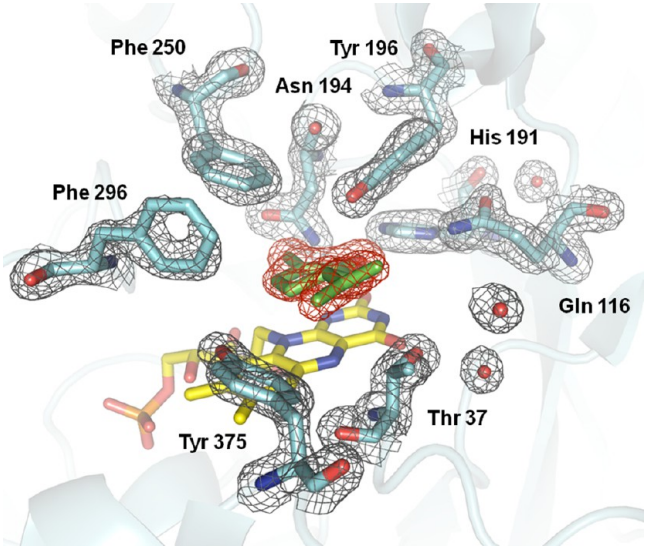

Figure 7. Structure of Trp 116 Gln OYE 1 complexed with (*R*)-carvone. The gray mesh shows the 2mFo-DFc electron density map contoured at the 1.2 σ level for key protein residues, and the red mesh shows the omit mFo-DFc maps at the 3 σ level for the ligand. Protein residues are colored in cyan and FMN in yellow.

other OYE 1 structure (Figure 6).[31] While the major conformer of Asn 194 was identical to that observed previously, the second placed the side-chain carbonyl above the FMN, occupying the same space normally filled by a chloride ion in an "empty" OYE 1 structure. Modeling only the two conformations of Asn 194 led to a positive peak in the $F_o - F_c$ difference map, which could be eliminated by adding a water molecule ion whose occupancy mirrored that of the Asn 194 side-chain in its usual conformation. It is possible to model a hydrogen bond network between the side-chain of Thr 116, WAT 723 and the side-chain of Asn 194 (in the second conformation), and these favorable interactions may partially explain the observed structural changes (Figure 6). It should be noted that locating the side-chain of Asn 194 directly above the FMN would preclude substrate binding, and this may be the reason that this Trp 116 variant showed poor catalytic efficiency.

Trp 116 Gln Mutant. The final mutant selected for structural studies was the Trp 116 Gln variant since this protein showed good catalytic activity toward both (*R*)- and (*S*)-carvone with altered stereoselectivity for the latter (Figure 1). In this regard, its properties closely resemble that of the Ile mutant. We were unable to determine a carvone oxidation activity for the Gln mutant, either because it was unable to catalyze the reaction or it was unable to form a stable charge-transfer complex carvone oxidation product **7** under our experimental conditions

Attempts to observe (*S*)-carvone within the active site of the Trp 116 Gln mutant by soaking with neat ligand were unsuccessful and the active site electron density observed corresponded to a chloride ion. Soaking experiments with (*R*)-carvone did afford a complex; however, there were several unusual features (PDB code 3TXZ). Based on the stereochemistry of its reduction, we anticipated a "normal" substrate binding orientation similar to that seen for the wild-type and Leu variant. Instead, the substrate was observed in a "flipped" orientation, which would lead to the opposite stereoisomer (Figure 7).

Several features of this "flipped" complex argue that it does not represent a catalytically productive arrangement. First, the distances between the substrate's carbonyl oxygen and $N\epsilon 2$ of His 191 and $N\delta 2$ of Asn 194 were 3.7 and 4.6 Å, respectively. Such distances preclude hydrogen bonds, which are known to be essential for catalytic turnover by OYE 1.[32] An analogous binding mode for phenols, lacking these hydrogen bonds, would also be consistent with our inability to observe a charge-transfer complex in dismutation studies of the Gln mutant. In wild-type OYE 1, a hydrogen bond between the phenol oxygen and the side-chain of His 191 stabilizes the former in its electron-rich anionic form, allowing a charge-transfer complex with the electron-deficient FMN.[32] By mutating His 191, Massey demonstrated that loss of this hydrogen bond eliminated charge-transfer complex formation; in our case, it is ligand repositioning that eliminates the interaction.

The geometric relationship between bound (*R*)-carvone and the FMN cofactor also argues against the catalytic relevance of the observed complex. In particular, the angle formed between C_β of carvone and the plane of the FMN is 66.5°, well outside the range observed by Fraaije in his survey of flavoproteins bound to their respective substrates and/or products,[17] strongly suggesting that hydride transfer would be impossible from such a geometry. Interestingly, the carbonyl of (*R*)-carvone is positioned between the side-chains of His 191 and Gln 116, reminiscent of its normal location between His 191 and Asn 194.

Understanding Stereocontrol by OYE 1. Our goals in this study were to uncover general principles by which the orientation of substrate binding was controlled in enzymes of the OYE superfamily and also to generate proteins that selectively provided synthetic access to all four possible carvone reduction products. Given the hydrophobic character of carvone (and most other alkene reductase substrates of synthetic interest), we hypothesized that substrate binding orientation would be controlled largely by steric factors. Consistent with this notion, the OYE 1 active site is largely composed of uncharged amino acid side-chains.

Our crystallographic studies provided experimental data for all four possible types of OYE 1/ligand complexes: carvone

dx.doi.org/10.1021/cs400622e | *ACS Catal.* 2013, 3, 2376−2390

bound in the "normal" orientation, carvone oxidation product 7 in the "normal" orientation, carvone bound in the "flipped" mode, and phenol 7 in the "flipped" mode. To obtain an unbiased, comparative view of substrate binding, all of these structures were superimposed using only the FMN moieties (Figure 8A). With a few exceptions noted above, protein residues for all structures occupied essentially the same locations in the overlaid structures. Regardless of the ligand oxidation state or binding orientation, all ligands placed their oxygen atoms at a common point that lies within hydrogen bonding distance of His 191 and Asn 194. This convergence reinforces the notion that this interaction is highly important to ligand binding.[33]

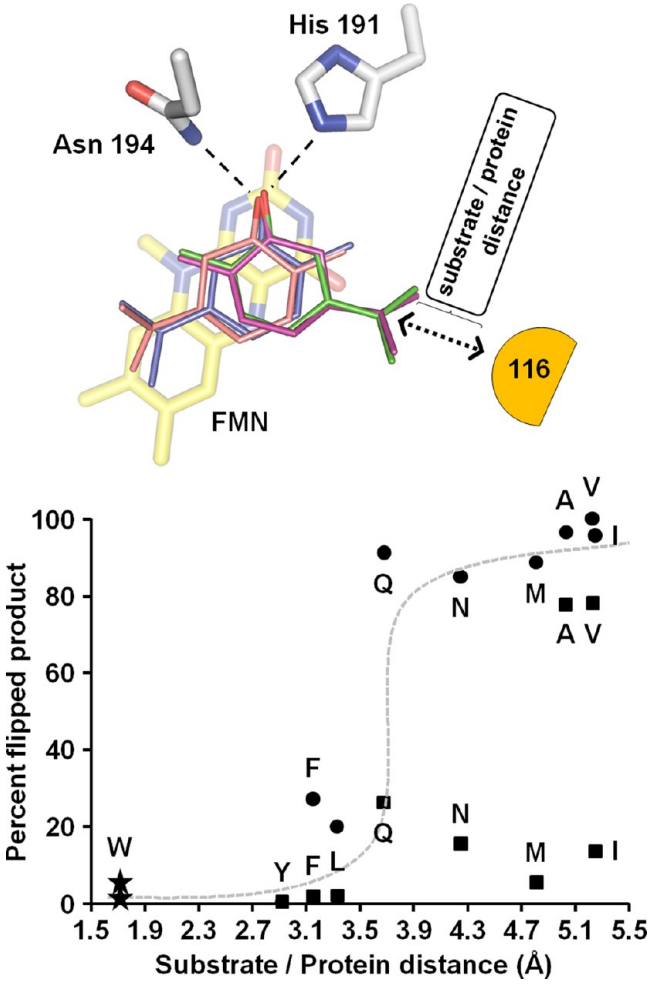

Figure 8. The influence of steric interactions on "flipped" substrate binding by wild-type and Trp 116 OYE 1 variants. (**A**) Overlay of ligand positions determined from X-ray crystallography studies. Structures of OYE 1 variants with the carvone oxidation product 7 in the "normal" binding mode (Trp 116 Leu, PDB code 4GXM, blue), phenol 7 in the "flipped" binding mode (Trp 116 Val, PDB code 4H4I, green), (*R*)-carvone in the "normal" binding mode (Trp 116 Leu, PDB code 4GWE, pink), and (*S*)-carvone in the "flipped" binding mode (Trp 116 Ile, PDB code 4GE8, purple) were overlaid using the FMN coordinates. In all cases, the oxygen atoms lay in essentially identical positions, where they could interact with the side-chains of His 191 and Asn 194. The distance from the central carbon of the side-chain propenyl carbon to the closest atom of the side-chain at position 116 is indicated schematically. (**B**) Correlation between substrate/protein distance and carvone binding in the "flipped" orientation. Distances between the bound substrate and the side-chain at position 116 were determined as described in the text and plotted against the percentage of product arising from the "flipped" substrate binding orientation for both (*S*)- (●) and (*R*)-carvone (■).

Interestingly, whether the ligand was aromatic or non-aromatic, the positions of the branchpoint carbons of the side-chains (C_8) were essentially identical (Figure 8A). While the positions of these atoms were well-defined, the terminal methyl and methylene moieties (C_9 and C_{10}, respectively) likely occupied a range of locations because of facile rotation around the C_5-C_8 bond at noncryogenic temperatures. We attempted to correlate the results of catalytic assays, particularly the extents of carvone oxidation and the propensity for substrate binding in the "flipped" orientation prior to alkene reduction, with a variety molecular distances and angles obtained from the aggregated crystal structures. The most informative comparison turned out to be the distances between the ligand C_8 atom and the closest atom of the side-chain at position 116.[34] For Trp 116 variants that bound 7 in the "flipped" orientation (Ala and Val), these distances could be measured directly from the X-ray structures. In cases where protein crystal structures were known, but no "flipped" ligand complexes had been observed experimentally (wild-type, Ile and Gln), phenol 7 was modeled into the active sites based on the structural alignment in Figure 8A. Finally, for those Trp 116 variants lacking crystal structure data (Asn, Met, Phe, and Tyr), both the altered side-chain and the phenol 7 in the "flipped" binding orientation were modeled.

We found a good correlation between the interatomic distances separating 7 and the closest atom of the position 116 side-chain and the fraction of carvone reduction product derived from the "flipped" binding orientation (Figure 8B). The relationship was consistent for (*S*)-carvone: if the ligand/protein distance was less than about 3.7 Å, the enzyme was unable to bind this substrate productively in the "flipped" orientation. Given the *C*-*C* bond distances between C_8, C_9, and C_{10} and the angular rotation of the side-chain, this critical distance likely reflects complexes that would have had ligand/protein complex distances below the van der Waals contact limits. This is consistent with the notion that control of substrate binding orientation is largely steric in origin.

Three Trp 116 variants showed significant deviations from the predicted behavior for (*R*)-carvone (Asn, Ile, and Met); in each case, additional factors likely contribute. Our crystallographic studies of the Trp 116 Gln mutant revealed that this side-chain provoked an unusual substrate binding mode, and it is possible that the Asn side-chain caused similar perturbations. In the case of the Ile variant, binding of (*S*)-carvone caused partial repositioning of the isobutyryl side-chain to accommodate the substrate and some disorder was apparent in this residue. These observations suggest that the mutant only reluctantly allows (*S*)-carvone binding in the "flipped" orientation, and that the steric interactions are close to unallowable in this case. Subtle differences in side-chain positions between (*S*)- and (*R*)-carvone would be expected from the difference in cyclohexene ring half-chair conformations preferred by the two substrate enantiomers. These small differences were erased in the modeled complex with phenol 7 used to construct the relationship in Figure 8A. Finally, the orientation(s) of the Met side-chain at position 116 are highly uncertain because of the numerous accessible χ values for this residue, which lead to significant uncertainties in predicting the appropriate distance between this side-chain and the C_8 atom of phenol 7.

dx.doi.org/10.1021/cs400622e | *ACS Catal.* 2013, 3, 2376−2390

The most striking conclusion from this work is that OYE 1's preferred binding mode for carvone is actually the "flipped" orientation. Only when this arrangement is sterically forbidden does the enzyme accept the alternative, "normal" binding mode. While the term "normal" was chosen because it describes the behavior of the wild-type enzyme, our data show that this substrate binding arrangement is actually less preferred. Replacing Trp with smaller residues such as Ala or Val created additional volume on one side of the active site, but the opposite side remained the same as in the wild-type. Both variants should therefore have had sufficient space to bind the substrate in either orientation, and the *in crystallo* oxidation of (+)-dihydrocarvone strongly supports this contention. Thus, if both orientations were sterically accessible, why was only one strongly preferred? Our crystallographic studies have provided one possible explanation. When carvone is bound in the "normal" orientation, its isopropenyl side-chain projects into a pocket partially defined by the side-chains of Phe 250, Phe 296, and Tyr 375 (Figure 3D). The structure of the Trp 116 Leu variant complexed with (*R*)-carvone showed that the side-chains of both Phe 296 and Tyr 375 had to move from their preferred positions in the apoprotein to accommodate the substrate. By contrast, in the "flipped" substrate binding orientation, the side-chain of carvone projects into a pocket lined entirely by hydrophobic protein residues,[35] none of which show significant reorientation upon substrate binding (Figure 5B). The better match between the hydrophobic side-chain of carvone and the newly created binding pocket on the "eastern" side of the active site is a second reason that the enzyme might prefer the "flipped" binding orientation. From this perspective, the "normal" substrate binding mode for carvone is forced upon wild-type and some OYE 1 variants as the only way to avoid steric overlap between the substrate side-chain and the residue at position 116, despite being disfavored by the need to reorient Phe 296 and Tyr 375. In the case of wild-type OYE 1, the sheer size of the indole ring overrides all other considerations. Substituting smaller groups for this side-chain unmasks the enzyme's intrinsic preference for the alternative substrate binding mode. The active site surfaces of the wild-type and the Trp 116 Val variant illustrate these differences in binding pockets clearly (Figure 9). The indole ring of Trp 116 acts as a "gate" that blocks access to one side of the active site; once the blockade has been lifted, a hydrophobic pocket that can accommodate larger substrates becomes accessible. Moreover, given the high sequence and structural homology between OYE family members, it is unlikely that the phenomena uncovered here are confined to the *S. pastorianus* enzyme, and similar approaches may also yield useful variants of other enzymes in the alkene reductase family of biocatalysts.

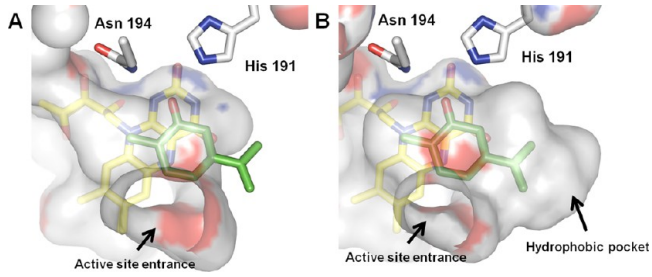

Figure 9. Active site surfaces. (**A**) (*R*)-carvone modeled (green) in the "flipped" binding orientation within the active site of wild-type OYE 1. The ligand position was based on experimental data from the Ala and Val variants and preserves the hydrogen bond between the carbonyl oxygen and the side-chains of His 191 and Asn 194. The interior active site surface (calculated with a probe sphere of 1.4 Å radius) is shown semitransparently, and the entrance to the active site is indicated by an arrow. The side-chain of Trp 116 lies on the right side of the active site and precludes this modeled "flipped" substrate binding orientation. (**B**) Active site surface of the Trp 116 Val OYE 1 with bound (*R*)-carvone **4** (green) (PDB code 4K8H). The interior active site surface (calculated with a probe sphere of 1.4 Å radius) is shown semitransparently, and the entrance to the active site is indicated by an arrow. A hydrophobic pocket that can accommodate the isopropenyl side-chain of **4** is highlighted.

EXPERIMENTAL SECTION

Carvone Reductions. Wild-type and OYE 1 variants with all possible amino acids at position 116 were overexpressed as fusion proteins with glutathione *S*-transferase in *E. coli* and purified by affinity chromatography as described previously.[15] Screening reactions (300 μL total volume) were carried out in 50 mM KP_i, pH 7.5 containing 200 mM glucose, 25 U/mL GDH102 (BioCatalytics), 0.3 mM $NADP^+$, 10 mM carvone, and approximately 100 μg of purified GST-fusion protein. Reactions were shaken at room temperature for 16 h, then extracted with 500 μL of EtOAc. After brief centrifugation, aliquots of the organic layer (300 μL) were removed and analyzed by GC/MS (EI at 70 eV) using a 0.25 mm × 30 m DB-17 column with an initial temperature of 90 °C followed immediately by a 10 °C/min increase to 130 °C, a 2 °C/min increase to 150 °C, and a final increase of 20 °C/min to 250 °C (maintained for 5 min). Typical retention times were 7.23 min for the *trans*-(2*R*,5*R*) and -(2*S*,5*S*) reduction products, 7.62 min for the *cis*-(2*S*,5*R*) and -(2*R*,5*S*) reduction products and 8.84 min for the substrates.

Carvone Oxidations. Purified OYE 1 Trp 116 variants were diluted to about 15 μM in 100 mM KP_i, pH 8.0 and a final volume of 250 μL. The actual enzyme concentration used in each assay was calculated spectrophotometrically using FMN absorbance (ε^{462} = 11,700 M^{-1} cm^{-1})[32] and initial values for A^{462}, A^{648}, and A^{820} were recorded. Substrate (either (*R*)- or (*S*)-carvone) was added to a final concentration of 2 mM (from a 100 mM stock solution in EtOH). The mixtures were gently agitated at room temperature in a rotatory apparatus in sealed microcentrifuge tubes. After 24 h, the tubes were centrifuged for 2 min at room temperature, and UV−vis spectra were collected to provide final values for A^{462}, A^{648}, and A^{820}. In separate experiments, each variant was incubated for 2 min with 3 mM *p*-chlorophenol, then centrifuged and analyzed by UV−vis spectroscopy in the same manner as described above.

All values of A^{462} and A^{648} were corrected for small baseline variations by subtracting the A^{820} obtained for that spectrum. Data from incubations with *p*-chlorophenol were treated similarly. The initial A^{462}/A^{648} ratio reflected the optical properties of an OYE 1 with no phenol bound and the corrected final A^{462}/A^{648} ratio observed in the presence of excess *p*-chlorophenol provided the optical properties of the fully phenol-complexed protein. The fractional saturation of phenol binding derived from carvone oxidations after 24 h were calculated for the wild-type and selected mutant proteins using eq 1.

dx.doi.org/10.1021/cs400622e | *ACS Catal.* 2013, 3, 2376−2390

$$\%\text{phenol complex} = -\left(\frac{\text{corrected } A^{462}/A^{648}(24\text{ h})_{\text{carvone}} - \text{corrected } A^{462}/A^{648}{}_{p\text{-chlorophenol}}}{\text{corrected } A^{462}/A^{648}(0\text{ h})_{\text{carvone}} - \text{corrected } A^{462}/A^{648}{}_{p\text{-chlorophenol}}}\right) \quad (1)$$

Mutagenesis and Protein Isolation for Crystallography. Prior to crystallization studies, Trp 116 mutations were introduced into an overexpression plasmid for native OYE 1 (pET3b-OYE, a generous gift from Dr. Betty Jo Brown, University of Michigan)[36] using previously described methods.[15] Wild-type and Trp 116 mutant OYE 1 variants were purified by affinity chromatography[21] followed by gel filtration (Superdex 200) as reported earlier.[15]

Crystallogenesis and Data Collection. Crystals were obtained using a hanging drop vapor diffusion method at 4 °C. The protein concentrations were approximately 40 mg/mL in 50 mM Tris·HCl, 50 mM NaCl, 10 μM PMSF, pH 7.5 and the reservoir solution contained 35% PEG 400, 200 mM $MgCl_2$, 100 mM HEPES, pH 8.3. For crystal growth, equal volumes (ca. 5 μL) of the protein stock and reservoir solution were mixed and applied to a silanized glass coverslip. Crystals grew as yellow tetragonal rods and were typically observed initially after 5−7 days with continued growth over the next 7−14 days. Those chosen for data collection measured approximately 180 μm × 180 μm × 600 μm and diffracted to 2.0−1.3 Å resolution. For substrate soaking experiments, crystals were soaked in mother liquor containing saturated solutions of ligand for varying periods of time at 4 °C. Data collection was performed under cryogenic conditions at 100 K at Brookhaven National Laboratory beamlines X6A, X25, or X26C. Crystals were mounted on nylon loops and plunged into liquid nitrogen prior to data collection. When possible, resolution limits were set based on the signal-to-noise ratio in the highest resolution shell. In some cases, for example, 4GWE, physical limitations of the detection apparatus precluded a location sufficiently close to avoid data being lost beyond the edge of the detector, and the resolution limit was therefore governed by the physical position and dimensions of the detector.

***In Crystallo* UV−vis Spectroscopy.** Data were collected at National Synchrotron Light Source (NSLS) X26C beamline in Brookhaven, NY. This beamline is equipped with a microspectrophotometer (350−800 nm) with an approximately 25 μm diameter optical focal point focused on the crystal rotation axis. The source objective that focuses the light from a 75 W Xe arc lamp onto the sample is mounted above the sample, allowing absorption spectra to be collected from protein crystals in conjunction with X-ray diffraction data. For concurrent spectroscopy collection, the crystal was oriented with its flat face normal to the spectroscopy photons. Spectra were measured at 5° intervals over a 360° rotation, and the characteristic spectral peaks determined for OYE 1 in solution (384 and 462 nm) were analyzed with respect to the crystal orientation. Electronic absorption and X-ray diffraction data collection were integrated into the data collection software (CBASS). For example, during the X-ray detector readout, the crystal was rotated to the optimal crystal orientation angle, a spectrum was collected, and the crystal was returned to the correct orientation for X-ray data collection. Thus, all spectra collected for a particular crystal were from the same orientation of the crystal. We did not attempt to estimate the absorbed X-ray dose since no substantial changes were detected in the UV−vis spectral region of interest. Additionally, no significant deterioration was noticed in the X-ray diffraction data throughout the experiment.

Structure Solution. X-ray data sets were processed using HKL2000[37] or iMOSFLM.[38] Structures were solved by molecular replacement using AUTOMR in the PHENIX suite.[39] The search used a high resolution structure of OYE 1 (PDB codes 1OYB[10] or 3RND[15]) devoid of water molecules and any ligands; in addition, residue 116 was initially modeled as an alanine. Inspection of the electron density maps was followed by manual rebuilding, addition of ordered waters, and refinement of each model's coordinates and temperature factors against the X-ray data. During refinement, inspection of the calculated $2F_o - F_c$ and the $F_o - F_c$ difference map showed clear positive electron density for the side chain of residue at position 116 and for bound ligands above the isoalloxazine moiety of the bound FMN cofactor. This allowed for building of the correct residue 116 side chains and unambiguous placement of the nonprotein ligands. This process was performed iteratively until residual errors R_{work} and R_{free} converged.

Modeling of OYE 1/Phenol 7 Complexes Not Observed Experimentally. The coordinates for phenol 7 were modeled into the active sites of the wild-type, Asn, Gln, Met, Phe, Pro, and Tyr OYE 1 variants in a "flipped" orientation. The altered side-chains at position 116 were generated manually using COOT,[40] and their initial positions were selected based on the likelihood of observing a particular rotamer and when possible, similarity to a side-chain in an existing crystal structure model, for example, the side-chain of Phe was placed similarly to that of Trp.

The location of phenol 7 within the active site was constrained by hydrogen bond interactions with the $N\varepsilon_2$ and $N\delta_2$ atoms of His 191 and Asn 194, respectively, and also by distances from the FMN isoalloxazine ring and the side-chain of distance to the proton donor, Tyr 196. Using this information and the ligand positions observed experimentally in the crystal structures of the Ala and Val mutants, phenol 7 was manually placed into the active sites of the modeled OYE 1 variants. The resulting enzyme−inhibitor models were subjected to all-atom geometry optimization/energy minimization using REFMAC5[41] prior to manual inspection. Complexes in which the phenolic oxygen moved by ≥0.20 Å were discarded since they would likely represent unproductive complexes. This was the case for both the wild-type and the Trp 116 Tyr variant, so simple least-squares superposition was used to estimate steric clashes. Finally, the modeled Trp 116 Pro variant was not used in this analysis since all attempts to employ energy minimization failed. This may be due to backbone rearrangements that might be provoked by this substitution.[42]

AUTHOR INFORMATION

Corresponding Author

*E-mail: jds2@chem.ufl.edu. Phone: 352.846.0743. Fax: 352.846.0743.

Notes

The authors declare no competing financial interest.

■ ACKNOWLEDGMENTS

Financial support by the National Science Foundation (CHE-1111791) is gratefully acknowledged. We thank Dr. Colin Conerly for initially creating many of the Trp 116 mutants employed in this study and for some preliminary studies. We also thank Professors Steven Bruner and Robert McKenna (University of Florida) for helping us initiate the crystallographic studies as well as with Drs. Jean Jakoncic and Edwin Lazo, Dr. Annie Héroux and Drs. Allen M. Orville and Feifei Li for their assistance in data collection at the X6A, X25, and X26C beamlines, respectively. Financial support for National Synchrotron Light Source comes principally from the Offices of Biological and Environmental Research and of Basic Energy Sciences of the U.S. Department of Energy, and from the National Center for Research Resources (P41RR012408) and the National Institute of General Medical Sciences (P41GM103473) of the National Institutes of Health.

■ REFERENCES

(1) (a) Winkler, C. K.; Clay, D.; Davies, S.; O'Neill, P.; McDaid, P.; Debarge, S.; Steflik, J.; Karmilowicz, M.; Wong, J. W.; Faber, K. *J. Org. Chem.* **2013**, *78*, 1525−1533. (b) Fryszkowska, A.; Toogood, H.; Sakuma, M.; Gardiner, J. M.; Stephens, G. M.; Scrutton, N. S. *Adv. Synth. Catal.* **2009**, *351*, 2976−2990. (c) Gao, X.; Ren, J.; Wu, Q.; Zhu, D. *Enzyme Microb. Technol.* **2012**, *51*, 26−34. (d) Iqbal, N.; Rudroff, F.; Brigé, A.; Van Beeumen, J.; Mihovilovic, M. D. *Tetrahedron* **2012**, *68*, 7619−7623. (e) Oberdorfer, G.; Gruber, K.; Faber, K.; Hall, M. *Synlett* **2012**, *23*, 1857−1864. (f) Richter, N.; Gröger, H.; Hummel, W. *Appl. Microbiol. Biotechnol.* **2011**, *89*, 79−89. (g) Schittmayer, M.; Glieder, A.; Uhl, M. K.; Winkler, A.; Zach, K.; Schrittwieser, J. H.; Kroutil, W.; Macheroux, P.; Gruber, K.; Kambourakis, S.; Rozzell, J. D.; Winkler, M. *Adv. Synth. Catal.* **2011**, *353*, 268−274. (h) Müller, A.; Hauer, B.; Rosche, B. *Biotechnol. Bioeng.* **2007**, *98*, 22−29.

(2) Vaz, A. D. N.; Chakraborty, S.; Massey, V. *Biochemistry* **1995**, *34*, 4246−4256.

(3) Meah, Y.; Massey, V. *Proc. Natl. Acad. Sci. U.S.A.* **2000**, *97*, 10733−10738.

(4) Warburg, O.; Christian, W. *Naturwissenschaften* **1932**, *20*, 980−981.

(5) Mugford, P. F.; Wagner, U. G.; Jiang, Y.; Faber, K.; Kazlauskas, R. J. *Angew. Chem., Int. Ed.* **2008**, *47*, 8782−8793.

(6) Stueckler, C.; Hall, M.; Ehammer, H.; Pointner, E.; Kroutil, W.; Macheroux, P.; Faber, K. *Org. Lett.* **2007**, *9*, 5409−5411.

(7) Formerly known as *Saccharomyces carlsbergensis*.

(8) Swiderska, M. A.; Stewart, J. D. *J. Mol. Catal. B: Enzym.* **2006**, *42*, 52−54.

(9) Bougioukou, D. J. Ph.D. Thesis, University of Florida, Gainesville, FL, 2006.

(10) Fox, K. M.; Karplus, P. A. *Structure* **1994**, *2*, 1089−1105.

(11) (a) Bougioukou, D. J.; Kille, S.; Taglieber, A.; Reetz, M. T. *Adv. Synth. Catal.* **2009**, *351*, 3287−3305. (b) Hulley, M.; Toogood, H. S.; Fryszkowska, A.; Mansell, D.; Stephens, G. M.; Gardiner, J. M.; Scrutton, N. S. *ChemBioChem* **2010**, *11*, 2433−2447. (c) Fryszkowska, A.; Toogood, H.; Sakuma, M.; Stephens, G. M.; Gardiner, J. M.; Scrutton, N. S. *Catal. Sci. Technol.* **2011**, *1*, 948−957. (d) Reich, S.; Hoeffken, H. W.; Rosche, B.; Nestl, B. M.; Hauer, B. *ChemBioChem* **2012**, *13*, 2400−2407.

(12) Classen, T.; Pietruszka, J.; Schuback, S. M. *ChemCatChem* **2013**, *5*, 711−713.

(13) Padhi, S. K.; Bougioukou, D. J.; Stewart, J. D. *J. Am. Chem. Soc.* **2009**, *131*, 3271−3280.

(14) (a) Goretti, M.; Turchetti, B.; Cramarossa, M. R.; Forti, L.; Buzzini, P. *Molecules* **2013**, *18*, 5736−5748. (b) Fu, Y.; Castiglione, K.; Weuster-Botz, D. *Biotechnol. Bioeng.* **2012**, *110*, 1293−1301. (c) Aquino, G. L. B.; Oliveira, B.; Didonet, C. C. M. *Biocatal. Biotrans.* **2012**, *30*, 455−458. (d) Silva, V. D.; Stambuk, B. U.; Nascimento, M. d. G. *J. Mol. Catal. B: Enzym.* **2012**, *77*, 98−104.

(15) Walton, A. Z.; Conerly, W. C.; Pompeu, Y.; Sullivan, B.; Stewart, J. D. *ACS Catal.* **2011**, *1*, 989−993.

(16) (a) Matthews, R. G.; Massey, V. *J. Biol. Chem.* **1969**, *244*, 1779−1786. (b) Matthews, R. G.; Massey, V.; Sweeley, C. C. *J. Biol. Chem.* **1975**, *250*, 9294−9298. (c) Abramovitz, A. S.; Massey, V. *J. Biol. Chem.* **1976**, *251*, 5327−5336.

(17) Fraaije, M. W.; Mattevi, A. *Trends Biochem. Sci.* **2000**, *25*, 126−132.

(18) This criterion excluded the Arg, Cys, Glu, Gly, Lys, Ser, and Thr mutants since they showed less than 30% conversion in NADPH-driven carvone reductions.

(19) Preliminary studies had shown that the charge-transfer bands from *p*-chlorophenol and **5** were essentially identical; the former was used here because it was commercially available.

(20) Three Trp 116 variants (Asp, Gln and Tyr) yielded higher A^{462}/A^{648} ratios after incubation with carvone for 24 h when compared with the initial values. This likely reflected an inability to form a charge-transfer complex with the phenolate and/or a phenol complex whose opticaly properties differed significantly from that of the wild-type.

(21) Abramovitz, A. S.; Massey, V. *J. Biol. Chem.* **1976**, *251*, 5321−5326.

(22) All of our structures showed a slightly different protein structure near the *C*-terminus than reported previously as well as an ordered Mg^{2+} ion. Aside from these minor differences, the overall structures reported here are highly similar to that of 1OYB.

(23) Attempts to grow protein crystals in the presence of (*R*)- or (*S*)-carvone failed.

(24) The dihydrocarvone sample contained a diasteromeric mixture at position 2, but contained only the (*R*)-stereochemistry at position 5.

(25) Since both of these structures were essentially identical to that of 1OYB, these data were not deposited in the PDB or listed in Tables 2 through 5.

(26) Fox, K. M.; Karplus, P. A. *J. Biol. Chem.* **1999**, *274*, 9357−9362.

(27) Karplus, P. A.; Fox, K. M.; Massey, V. *FASEB J.* **1995**, *9*, 1518−1526.

(28) Since the structure of the Trp 116 Ala mutant complexed to phenol **7** derived from (*S*)-carvone was identical, this structure was not refined to completion.

(29) Whether this change in substrate binding orientation involves dissociation and rebinding of (*R*)-carvone or if it can occur intramolecularly is unknown; however, the high external concentration of (+)-dihydrocarvone would diminish the chances of rebinding any (*R*)-carvone released to the bulk solution, suggesting that the latter pathway may be more likely.

(30) Because the other two structures were essentially identical to 4K7Y, we did not carry them to final refinement.

(31) The side-chain of the Thr at position 116 also appeared to occupy two different conformations.

(32) Brown, B. J.; Deng, Z.; Karplus, P. A.; Massey, V. *J. Biol. Chem.* **1998**, *273*, 32753−32762.

(33) This location is also the site of chloride ion binding.

(34) While the terminal atoms of the side-chain (C_9 and C_{10}) lie closer to the position 116 side-chain, their positions were uncertain at noncryogenic temperatures because of facile bond rotation around the ring/side-chain connection. We therefore adopted the distance to C_8 (which is well-defined) as a surrogate for the ligand side-chain position.

(35) Thr 37, Met 39, Phe 74, Gly 77, Tyr 82, Ala 85, and Leu 118.

(36) Saito, K.; Thiele, D. J.; Davio, M.; Lockridge, O.; Massey, V. *J. Biol. Chem.* **1991**, *266*, 20720−20724.

(37) Otwinowski, Z.; Minor, W. Processing of X-ray Diffraction Data Collected in Oscillation Mode. In *Methods in Enzymology*; Academic Press: San Diego, CA, 1997; Vol. *276*, pp 307−326.

(38) Battye, T. G.; Kontogiannis, L.; Johnson, O.; Powell, H. R.; Leslie, A. G. *Acta Crystallogr., Sect. D: Biol. Crystallogr.* **2011**, *67*, 271−281.

(39) Adams, P. D.; Afonine, P. V.; Bunkoczi, G.; Chen, V. B.; Davis, I. W.; Echols, N.; Headd, J. J.; Hung, L. W.; Kapral, G. J.; Grosse-Kunstleve, R. W.; McCoy, A. J.; Moriarty, N. W.; Oeffner, R.; Read, R.

J.; Richardson, D. C.; Richardson, J. S.; Terwilliger, T. C.; Zwart, P. H. *Acta Crystallogr., Sect. D: Biol. Crystallogr.* **2010**, *66*, 213−221.
(40) Emsley, P.; Lohkamp, B.; Scott, W. G.; Cowtan, K. *Acta Crystallogr., Sect. D: Biol. Crystallogr.* **2010**, *66*, 486−501.
(41) Murshudov, G. N.; Vagin, A. A.; Dodson, E. J. *Acta Crystallogr., Sect. D: Biol. Crystallogr.* **1997**, *53*, 240−255.
(42) We observed that the Trp 116 Pro OYE 1 mutant was expressed at very low levels, consistent with the notion that its structural stability had been negatively impacted by the Pro substitution.
(43) Arg, Cys, Gly, Glu, Lys, Ser, Thr.
(44) Chen, V. B.; Arendall, W. B.; Headd, J. J.; Keedy, D. A.; Immormino, R. M.; Kapral, G. J.; W., M. L.; Richardson, J. S.; Richardson, D. C. *Acta Crystallogr., Sect. D: Biol. Crystallogr.* **2010**, *66*, 12−21.